# Quantitative Modelling of Microcalcification Detection in Digital Mammography

Andreas Rick, Serge Muller, Sylvie Bothorel, and Michel Grimaud

GE Medical Systems
283 rue de la Minière, 78533 Buc, France
Andreas.Rick@med.ge.com

**Abstract.** This article presents a simulation framework for the image acquisition on digital mammography systems. The framework is used to analyse the performance of a previously developed method for the detection of microcalcifications by a series of top-hat operators. The framework allows to determine the theoretical number of false positives and true positives for a given set of acquisition parameters and size of microcalcifications.
A minimal size of microcalcification that can be detected with sufficient certitude is analysed as a function of the pixel size of the detector and the acquisition conditions. An improved selection scheme for the detection threshold is developed which uses the model and the acquisition parameters to obtain a near-optimal detection for a wide range of acquisition conditions. Finally the model is evaluated on clinical images.

## 1 Introduction

Screening mammography is used today as the most important tool in the reduction of breast cancer mortality by early detection of the lesions. One of the early signs of breast cancer on mammography images are small depositions of radiologically very opaque materials like $Ca_3(PO_4)_2$, $CaCO_3$, $Mg_3(PO_4)_2$ which are called microcalcifications [9]. Many algorithms have been developed for their detection using a wide variety of methods like sub-band decomposition [1], fractals [2] or mathematical morphology [3][4]. When detecting microcalcifications we are facing the problem that their size has no lower limit and so their detection is always a compromise between detecting too much noise or missing very small calcifications. Some work has been done to estimate the noise level from the image itself [6], but this leads to an ambiguity of what is noise and what is image content. In our work we try to establish lower limits of the microcalcification detectability based on a model of the digital image chain. We use those limits for the selection of the local thresholds in our detection system for microcalcifications. In previous systems the selection of a threshold was often difficult as the noise is dependent on the image content. In this approach we can estimate the true and false positive rates as a function of the local thresholds and we can thereby optimise these thresholds to obtain the same compromise throughout the image. As the conditions of the image acquisition process are much more

C. Taylor, A. Colchester (Eds.): MICCAI'99, LNCS 1679, pp. 32–42, 1999.
© Springer-Verlag Berlin Heidelberg 1999

controlled for digital mammography system, as no film processing and scanning is required, high precision models can be used to perform a quantitative analysis of the breast tissue. Works have been done on mammography image normalisation [5] from digitalised films. Due to film processing and scanning process, the physical quantification is difficult but the results obtained are promising.

In section 2 we discuss the model of the image acquisition chain and include a brief description of the first stage of our previously published [3][4] detection system for microcalcifications.
In section 3 we analyse the systems performance for different sizes of microcalcifications, different pixel sizes and different doses.
In section 4 a new threshold selection method is derived from the model which allows an optimal distinction between microcalcifications and image noise for the whole range of acquisition parameters and tissue thicknesses.
Finally in section 5 we compare the theoretical detection rates with detection rates observed on clinical images acquired on a full-field digital mammography system.

## 2 Image Acquisition and Microcalcification Detection

A mammography image is obtained by a projection of X-rays through the breast. The X-rays are generated by the impact of electrons which are accelerated in a electric field ($\approx 30kV$) onto some anode material (Mo,Rh,W). The X-ray spectrum is a function of the anode material, the acceleration voltage and the angle of the rays relative to the anode.

The detector used for the mammograms analysed in this paper is a full-field digital mammography detector made of an amorphous silicon based photo-diode matrix which is covered with a $CsI$-scintillation screen which converts the X-rays to visible photons.

At any point in space the number $n(z, E)$ of direct X-rays of energy $E$ arriving from the source can be calculated from the initial spectrum $n_0(E)$ generated at the anode by integrating the attenuation along the path of the ray for all energies.

$$n(z, E) = \frac{n_0(E)}{z^2} \cdot e^{-\int_{l=0}^{z} \mu(l,E)dl} dE \tag{1}$$

### 2.1 Detector Model

Using the above model and the geometry of the acquisition, the number of photons $n(x, y, E)$ arriving on the surface of one pixel of the detector can be calculated:

$$n(x, y, E) = \frac{n_0(x, y, E)}{z^2} \cdot e^{-\int_{l=0}^{z} \mu(x,y,l,E)dl} dE \tag{2}$$

A detector model which describes the conversion of the X-rays to visible photons in the scintillation material and the conversion of the photons to charges in the photo-diodes and finally the conversion from charges to pixel counts is used to

link the number of X-ray-photons arriving at the entrance surface of a pixel $n(x, y, E)$ to the ideal pixel values $I_s(x, y)$.

$$I_s(x,y) = \int_0^{E_m} n(x,y,E) \cdot \eta(E) dE \tag{3}$$

The detector model basically contains a conversion efficiency $\eta(E)$ between the X-ray energy and the pixel value. The modulation transfer function of the scintillator material can be taken into account by applying a spatial filter to the pixel values $I_s(x, y)$. The scattered photons are currently not taken into account in this model, as most of the scattered radiation can be eliminated using an anti scatter grid. One can use a deconvolution processing to estimate the scatter component (see [5] [7]).

### 2.2 Noise Model

The noise analysis of the detector has shown two principal noise sources, the quantum noise of the x-rays and the electronic readout noise. In total we can approximate the noise by a Gaussian noise with a standard deviation dependent on the signal and on a constant $\sigma_e$ which represents the electronic noise.

$$\sigma_n(x,y) = \sqrt{\int n(x,y,E) dE + \sigma_e^2} \tag{4}$$

### 2.3 Model of the Breast

We assume that the breast is composed of adipose and fibrous tissue and that its thickness $l_b$ is know. Microcalcifications are modeled by a simple sphere of calcium inside the breast. To introduce this model in the detector model we replace the exponential term in equation 2 by a transmission term $t(x, y, E)$:

$$t(x,y,E) = e^{-\mu_b(E)\cdot l_b - (\mu_c(E) - \mu_b(E))\cdot l_c(x,y)} \tag{5}$$

where $\mu_b(E)$ and $\mu_c(E)$ are the attenuation coefficients of the breast tissue and of the calcification and $l_b$ and $l_c$ are the corresponding thicknesses. The $t(x, y, E)$ can be decomposed into two terms $t_b$ and $t_c$, one for the breast tissue and one for the additional attenuation of the calcification:

$$t(x,y,E) = t_b(x,y,E) \cdot t_c(x,y,E) \tag{6}$$

$$= e^{-\mu_b(E)\cdot l_b} \cdot e^{-(\mu_c(E) - \mu_b(E))\cdot l_c(x,y)} \tag{7}$$

In reality the breast tissue is not homogeneous but composed of different types of tissue. For a simulation any mixture of tissues can be considered, but in reality the only information about the tissue comes from the acquired image and therefore the exact decomposition into the different tissues is not possible. The decomposition becomes possible when only two different types of tissue are considered and the total thickness of the breast is known (see [5]).

### 2.4 Model of a Microcalcification

If we use a sphere with a radius $r$ to model a microcalcification, we obtain:

$$t_c(x, y, E) = e^{-(\mu_c(E)-\mu_b(E))\cdot\sqrt{r^2-x^2-y^2}} \tag{8}$$

It can be remarked that the position inside the breast in the direction of the x-rays has no influence on the microcalcification transmission but due to the conic projection the calcifications closer to the tube are slightly magnified. The system we used for the evaluation has a tube to detector distance of 66cm. Under these conditions and with a maximum compressed breast thickness of 10cm the maximal magnification is 14% which should be taken into account during the detection process.

### 2.5 Detection System for Microcalcifications

We previously used the top-hat operator in a multi-scale scheme for microcalcification detection [4]. The top-hat operator, which combines the opening and subtraction of an image, is well adapted to the detection of structures like microcalcifications that have a small size and a hight contrast.

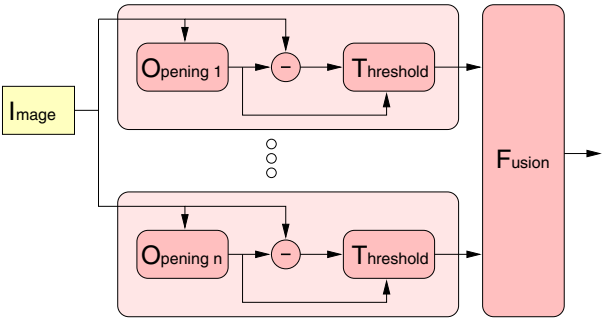


**Fig. 1.** Detection of microcalcifications using top-hat operators with different structuring element sizes

The opening removes all structures smaller than the structuring element from the image. The result of the subtraction from the original image gives only the small structures and a threshold is used to retain only the structures with a high contrast. As the sizes of the microcalcifications are not known in advance the top-hat operator is applied several times to the image using different sizes of structuring element and the result is combined (figure 1).

### 2.6 Overall Simulation Model

The simulation model shown in figure 2 can be constructed from the blocks described above. A number of parameters are fixed in each simulation, others (position of the calcification, threshold, noise) are modified statistically and a

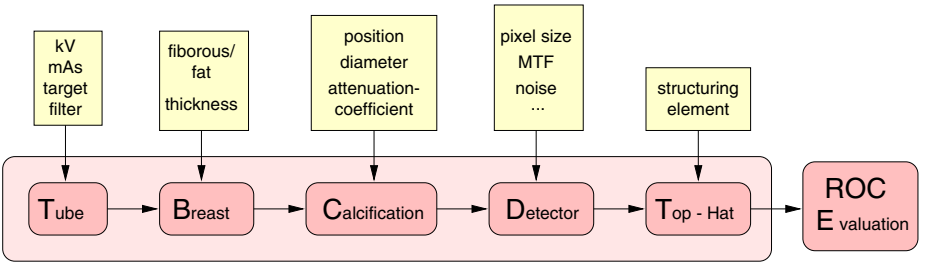


**Fig. 2.** Simulation model for the detection process

Receiver Operating Characteristic curve is calculated. This model is used in the following to analyse the performance of each top-hat operator used in the detection system for microcalcifications.

## 3 Applications of the Simulation Model

Our goal in this paper is to calculate the limits of detectability of microcalcifications using the detection process described above and to adapt the threshold and the fusion operator to obtain the best possible detection rate.

### 3.1 Influence of the Pixel Size

The model is used to analyse the effect of changing the pixel size with all other factors being constant (e.g. dose). Figure 3 shows how the area $A_z$ under the ROC curve changes for different sizes of microcalcifications. The conditions chosen are those of a dense breast (Rh/Rh, 30kV, 100mAs, 5cm). We observe that the detection quality globally increases with decreasing pixel size. At very high $A_z$ values the lines for 50 and 100 $\mu$ come very close (see top of figure 3 left). A useful computer aided detection system must achieve very high detection rates with little false positives and therefore it must have a high $A_z$ value. Under these constraints the smallest microcalcifications that can be detected are about 0.15 mm in dense regions of the breast. Reducing the pixel size below $100\mu m$ does not improve their detection.

For microcalcifications in adipose regions of the breast the detection performance $A_z$ increases with decreasing pixel size. For the same high level of $A_z$

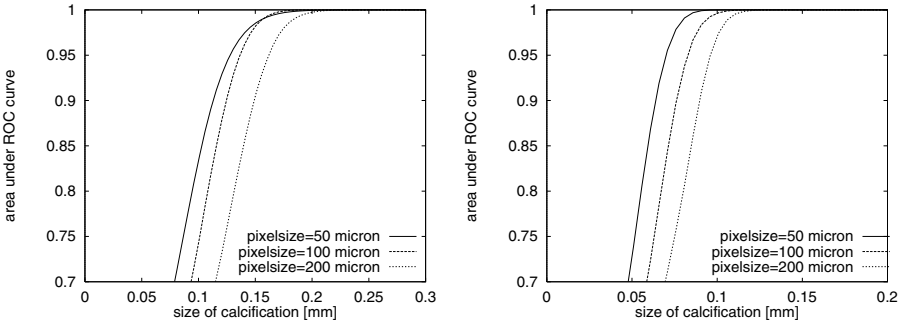


**Fig. 3.** Detection efficiency $A_z$ as a function of calcification size and detector pixel size for a dense breast (left) and adipose breast (right)

the smallest microcalcifications that can be detected are about 70 to 100$\mu m$ depending on the pixel size.

It is interesting to remark that the observer performance studies for the characterisation of malignant and benign microcalcification recently presented by Heang-Ping Chan [8] suggest the same optimum pixel size of either 70$\mu m$ or 105$\mu m$ and that 35$\mu m$ pixel size gives worse results - even though they did not achieve sufficient statistical evidence in their study yet.

### 3.2 Influence of Dose and Anode

The simulation model can also be used to calculate the influence of dose and anode/filter combination on the detectability of microcalcifications. We have chosen a dense breast and calculated the exposure (in mAs) necessary to obtain a detection performance given by an area under the ROC curve equal to 0.99 (figure 4). We can see that the Rh/Rh anode filter combination improves the microcalcification detectability in dense breasts. In addition, we can see that the dose must increase dramatically as the size of microcalcification to be detected decreases.

## 4 Model Based Selection of Thresholds

The number of false positives obtained by using a given threshold $t$ for the top-hat operator can be calculated using the noise model. For a Gaussian noise with standard deviation $\sigma_n$ as given in equation 4 the probability $\tilde{p}_{fpr}$ of a pixel value to be higher than the threshold $t$ for a given background value $bg$ is expressed by the integrated normal distribution:

$$\tilde{p}_{fpr}(x,y) = \int_{t+bg(x,y)}^{\infty} \frac{1}{\sqrt{2\pi}\sigma_n(x,y)} e^{-\frac{1}{2}\left(\frac{g-bg(x,y)}{\sigma_n(x,y)}\right)^2} dg \tag{9}$$

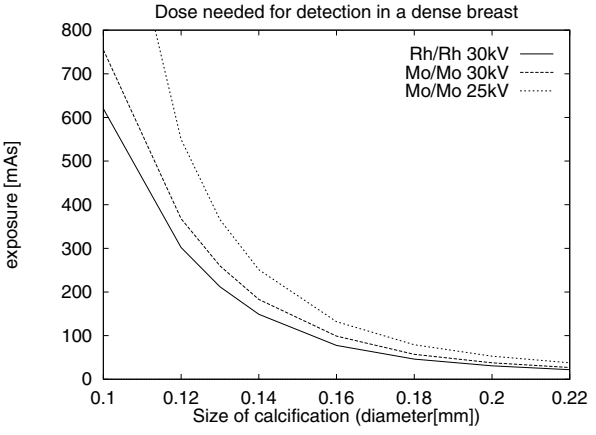


**Fig. 4.** Dose needed for detection of microcalcifications of different sizes using Mo or Rh anode with $A_z = 0.99$ in a dense breast

For all the $N$ pixels in the structuring element the probability of a false positive is given by:

$$p_{fpr}(x, y) = 1 - (1 - \tilde{p}_{fpr}(x, y))^N \tag{10}$$

The total number of false positives on a pixel basis is equal to the sum over all pixels of $p_{fpr}(x, y)$:

$$n_{fpr} = \sum_y \sum_x p_{fpr}(x, y) \tag{11}$$

The same reasoning can be applied for the calculation of the true positive rate for a spherical microcalcification of a given size.

Having calculated these detection rates we can choose an adapted detection strategy which represents a compromise between the true and false positives rates as a function of the microcalcification size and the image noise.

One strategy would be to select a constant true positive rate independent of the microcalcification size. Due to the higher image noise in the dense regions of the breast this leads to an unacceptably high false positive rate for small microcalcifications in these regions. The fusion stage which combines the results of the top-hats of different sizes must take into account this higher uncertainty for the small size top-hats.

A more interesting strategy is to give an a priori number of false positives coming from the combination of the top-hats and to select a number candidates from the top-hats until this selected number of false positive is reached. The block diagram for this approach is shown in figure 5.

For each size of the top hat operator, a number of false positives per pixel is estimated. For a given pixel, the threshold on the top-hat image which makes this pixel positive is used to estimate the number of false positives created by the

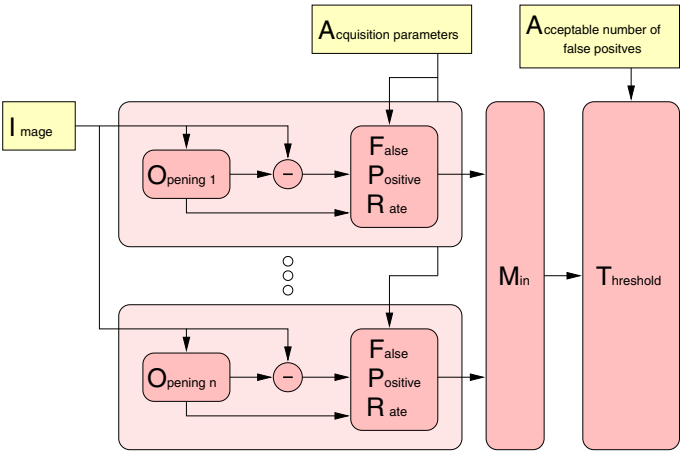


**Fig. 5.** Detection of microcalcifications using an estimated false positive rate per pixel

noise corresponding to the local background value. The different false positive rates are then combined using the minimum operator. This operator allows to mark those microcalcification candidates for which the best adapted top-hat operator results in the lowest false positive rate. Finally a global threshold is used to choose the pixels with the lowest possible false positive rate.

This method has the advantage to combine the information from the different sizes of top-hat operators by taking into account their confidence values in a very intuitive way.

## 5 Evaluation on Clinical Images

An evaluation of this false positive rate estimation was performed on clinical images from the GE Full Field Digital Mammography (FFDM) [11] system from two different clinical sites.

### 5.1 Theoretical versus Measured False Positive Rate

Using the acquisition parameters selected to acquire an image on the FFDM system, the theoretical probability of false positives as function of the background grey-level and the threshold applied on the top-hats has been calculated (figure 6 left). The top-hat detector has been applied on a real image and the number of positives has been counted as a function of background and threshold (figure 6 right).

For regions with a low background value (regions with constant breast thickness) the correspondence between the predicted false positive rate and the measured detection rates on a real image is good. This confirms our hypothesis,

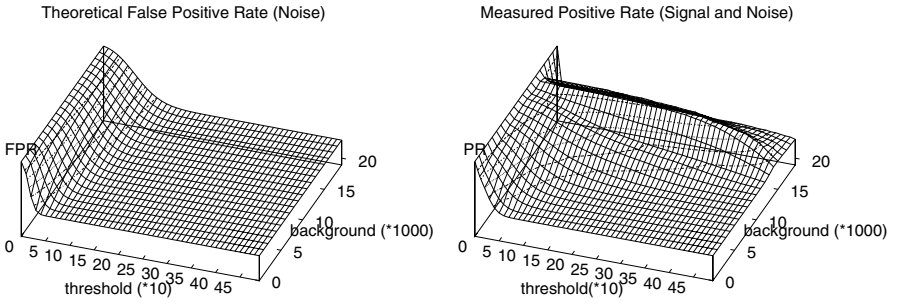


**Fig. 6.** Theoretical false positive rate(left) and measured positive rate (right)

that the detection problem inside the breast and especially for dense breasts is basically the problem of distinction from the image noise. For regions with high background values (breast border) the number of signal detected with higher thresholds is much higher than the predicted false positive rate due to noise. In these regions the dose arriving at the detector level is much bigger. It allows a much better distinction between breast structures and the noise is of lower importance. The detected structures are mostly fibrous structures and skin.

To distinguish fibrous structures from microcalcifications geometric or densitometric attributes can be used. Many algorithms about of false positives reduction have been published (e.g [10]). For illustration purpose, we show the effect of a densitometric constraint added to the detection process. The chosen constraint is a minimal attenuation coefficient for the detected structure which can be estimated from the size of the top-hat operator.

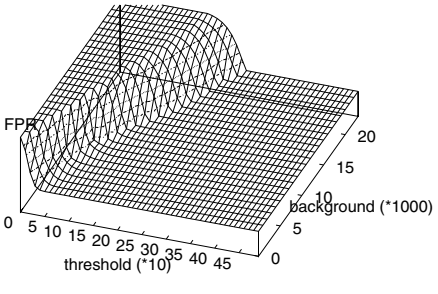


**Fig. 7.** Theoretical false positive rate including a densitometric constraint

The resulting theoretical false positive function shown in figure 7 is equal to the false positive function with noise only (figure 6) in dense regions (low background values) and exhibits a linear dependence between threshold and background values for higher background values. This allows to control the number of detected structures in the sub-cutaneous area.

## 6 Conclusions

In this paper we present a simulation system for the physics that underly the acquisition of images on digital mammography equipment. We use the model to calculate a minimal size of microcalcification that can be detected under given acquisition conditions and analyse the influence of pixel size and dose. The model is introduced in a detection system for microcalcifications to improve the detection performance across the different tissue thicknesses throughout the image. In addition, it becomes possible to calibrate the results relative to a theoretical false positive rate so that in order to obtain good detection results independently of the acquisition parameters. Finally we show that the correspondence between the theoretical false positive rate and the positive rate obtained on clinical images is good for regions inside the breast, where noise is the principal problem for the detection of calcifications.

## References

1. M. Nafi Gurcan, Yasemin Yardimci, A. Enis Cetin, Rashid Ansari, *Automated Detection and Enhancement of Microcalcifications in Mammograms Using Nonlinear Subband Decomposition*, Proceedings of IEEE ICASSP97, International Conference on Acoustics, Speech, and Signal Processing, April 20-24, 1997, München, Germany. 32
2. François Lefebvre, Habib Benali, René Gilles, Edmond Kahn, Robert Di Paola *A fractal approach to the segmentation of microcalcifications in digital mammograms*, Medical Physics, Vol. 22, No.4, April 1995, pp.381 - 390 32
3. Sylvie Bothorel, *Analyse d'image par arbre de décision floue - Application à la classification sémiologique des amas de microcalcifications en mammographie numérique*, Thèse de doctorat à l'université Paris 6, 1996 32, 33
4. Michel Grimaud, *La géodesie numérique en morphologie mathématique. Application à la détéction automatique de microcalcifications en mammographie numérique*, Thèse de doctorat à l'Ecole Nationale Supérieure des Mines de Paris, 1991 32, 33, 35
5. Ralph Highnam, Michael Brady, Brasil Shepstone *A representation for mammographic image processing*, Medical Image Analysis, Vol. 1, No.1, 1996, pp. 1 - 18 33, 34
6. Nico Karssemeijer, *Adaptive Noise Equalization and Recognition of Microcalcification Clusters in Mammograms*, in "State of the Art in Digital Mammographic Image Analysis", edited by K.W. Bowyer, S. Astley, World Scientific, 1994 32
7. J.M. Dinten, J.M. Volle, M. Darboux *Quantitative interpretation of mammogramms based on a physical model of the image formation process*, 4th International Workshop on Digital Mammography, Univerity of Nijmegen, The Netherlands, June 7-10, 1998 34

8. Heang-Ping Chan et.al. *Digital Mammography: Observer Performance Study of the Effect of Pixel Size on Radiologists Characterization of Malignant and Benign Microcalcifications*, SPIE Medical Imaging 99, International Conference on Acoustics, Speech, and Signal Processing, Feb. 20-26 1999, San-Diego, CA. USA. 37
9. Marton Lanyi, *Diagnosis and Differential Diagnosis of Breast Calcifications*, Springer Verlag 1986 32
10. Rufus H. Nagel, Robert M. Nishikawa, John Papaioanou, Kunio Doi, *Analysis of methods for reducing false positives in automated detection of clustered microcalcifications in mammograms*, Medical Physics, Vol. 25, No. 8, August 1998, pp. 1502 - 1506. 40
11. Serge Muller *Full-Field Digital Mammography designed as a complete system*, European Journal of Radiology, Invited Paper, to appear in 1999. 39